Journal of the European Ceramic Society 39 (2019) 3830–3836

Contents lists available at ScienceDirect

Journal of the European Ceramic Society

journal homepage: www.elsevier.com/locate/jeurceramsoc

Original Article

Fracture resistance of yttria stabilized zirconia manufactured from stabilizer-coated nanopowder by micro cantilever bending tests

S. Giese[a,*], F. Kern[b], C.A. Macauley[a], S. Neumeier[a], M. Göken[a]

[a] Friedrich-Alexander-Universität Erlangen-Nürnberg (FAU), Materials Science & Engineering, Institute I, Martensstr. 5, 91058 Erlangen, Germany
[b] Universität Stuttgart, Institut für Fertigungstechnologie keramischer Bauteile, Allmandring 7B, D- 70563 Stuttgart, Germany

ARTICLE INFO

Keywords:
TZP
Ceramic
Fracture toughness
Micro cantilever
Small scale

ABSTRACT

Yttria stabilized tetragonal zirconia polycrystal (Y-TZP) owes its high toughness to transformation toughening, a mechanism that requires the development of a process zone. It is important to measure if and to what extent the size of components can be reduced. In this study, tests were carried out using focused ion beam or picosecond milled pre-notched, 3 mol percent Y_2O_3 (3Y-) TZP micro-cantilever (10–250 μm) beams. The tests show clearly that the maximum fracture resistance is size dependent and the plateau toughness was not reached in any of the small-scale samples. A correlation between transformability of the tetragonal phase and the measured fracture resistance became visible only for the largest micro cantilever but did not reach the values measured in macroscopic samples. Based on these results, it is not advantageous to use very tough zirconia materials in components with dimensions smaller than ~0.25 mm, as the high toughness is not fully realized.

1. Introduction

Zirconia based structural ceramics are frequently applied in fields such as biomedical and mechanical engineering which require a combination of high strength and fracture resistance at ambient temperature. The excellent fracture resistance of zirconia, which has a very moderate crack tip toughness of only 3-4MPam$^{1/2}$ is due to "transformation toughening (TT)" a martensitic transformation of metastable tetragonal phase (t) to stable monoclinic phase (m) which is accompanied by volume expansion and shear [1,2]. In order to retain the metastable tetragonal phase after sintering, zirconia is stabilized with iso- or aliovalent metal oxides such as CeO_2, MgO or Y_2O_3 [3]. 3Y-TZP containing 3 mol-% Y_2O_3 is the most commonly used material in e.g. dental restorations [4]. At sintering temperature (typically 1300–1550 °C), this composition is located in the t + c field which represents a miscibility gap and should contain ~80% tetragonal and 20% cubic phase [5]. 3Y-TZP powders can be made by coprecipitation of zirconia and stabilizer which leads to a stabilizer supersaturated tetragonal material or by intense mixing of zirconia and stabilizer (either mechanical or by coating) [6,7]. State of the art coprecipitated 3Y-TZP can reach a strength > 1000 MPa and a toughness of 5–6 MPam$^{1/2}$ [4]. The mixed or coated 3Y-TZPs - which are applied in the current study – are non-equilibrium materials. At low sintering temperature and dwell times they retain a stabilizer gradient in the grain boundaries which results in high toughness (> 10 MPam$^{1/2}$) and excellent low temperature degradation stability [7–9].

The determination of the fracture resistance of ceramics can be quite challenging. Micro cantilever bending tests offer an alternative possibility to measure the mechanical properties of ceramics and to compare them with common testing techniques like Vickers or nanoindentation testing. Recent studies of Turon-Vinas et al., investigated the possibility to produce sharp notches with a laser abrasive method in 3 mol.-% yttria doped zirconia for determining fracture toughness [10]. In the present work, the fracture toughness of Y-TZP will be investigated with micro cantilevers produced by picosecond laser and focused ion beam (FIB) milling methods, in- and ex-situ test setups and digital image correlation (DIC) [11,12]. The advantages of these methods are that the local intrinsic fracture toughness of the material can be measured precisely with very sharp initial cracks at the micro scale [13]. Raman spectroscopy is used to investigate the transformation toughening effect at the fracture surface of micro cantilevers of specimens sintered at different temperatures.

In the case of tetragonal zirconia, the transformation toughening effect must be considered in addition to the intrinsic toughness. Different models have been proposed, among them the models by Budiansky and by McMeeking are the most prominent [14,15]. It is assumed that a phase transformation of the metastable tetragonal phase is initiated once a critical stress is reached. Initially at infinitesimal

* Corresponding author.
E-mail address: sven.giese@fau.de (S. Giese).

https://doi.org/10.1016/j.jeurceramsoc.2019.05.006
Received 21 January 2019; Received in revised form 3 May 2019; Accepted 4 May 2019
Available online 05 May 2019

crack growth, a cardioid transformed zone with a height h is formed in which the increase in stress intensity at +/- 60° ahead of the crack tip is exactly equilibrated by the reduced stress intensity in the remaining +/- 120°. It is therefore assumed that the initial zone has no effect on toughness. Toughening occurs as soon as the crack grows and it can be accepted that the plateau toughness is reached once the crack length has reached a length $a_s = 5\,h$. Moreover it should be noted that all models imply that the material reacts fully elastic and that the process zone is significantly smaller than the sample size.

2. Experimental methods

2.1. Manufacturing and characterizing the 3Y-TZP specimens

3Y-TZP starting powder was prepared by coating a monoclinic zirconia nanopowder ($S_{BET} = 15 m^2/g$) with yttrium oxide via the nitrate route by a modified procedure first described by Yuan [16]. The process is described in detail elsewhere [9]. 0.5 vol.-% of alumina was added to enhance sinterability and low temperature degradation (LTD) stability. The powder mixture (250 g) was milled in 300 ml 2-propanol with 3Y-TZP milling balls (Ø = 2 mm) for 2 h. The dispersion was subsequently dried after removal of the milling media and screened through a 100 µm mesh. The semi-finished samples for machining of micro cantilever tests (d = 22 mm, h = 2.5 mm) were consolidated by hot pressing (FCT Anlagenbau, Germany) in a graphite die at 1300 °C, 1375 °C and 1450 °C for 1 h at 50 MPa axial pressure. Samples were afterwards ground and polished prior to micro cantilever preparation. For the macroscopic samples, larger disks of 40 mm diameter were hot pressed under identical conditions. The sample preparation and test schedule (mechanical testing, XRD, microstructure) were explained in detail elsewhere [9]. To compare identical materials, a fresh set of macroscopic samples made from the same powder as for the microsamples was produced and measured.

Mechanical characterization included measuring of the Vickers hardness HV10 (Bareiss, Germany) and the determination of the Young's modulus E by impulse excitation technique of an entire polished disk of 40 mm diameter and 2 mm thickness (IMCE, Belgium). Fracture resistance K_{DCM} was measured by two indenter-based methods. Direct crack length measurement (DCM) of cracks induced by HV10 indents was carried out and the toughness was evaluated according to the formula of Niihara for Palmqvist cracks (5 indents each) [17,18]. Indentation strength in bending (ISB) tests were performed by notching polished bending bars (4 bars each) with HV10 indents placed in the middle axis of the sample with the wing cracks parallel and perpendicular to the sides. Special care was taken to produce HV10 indents with 4 fully developed wing cracks. The residual strength of the sample was then immediately measured in a 4-point setup with 20 mm outer and inner span (crosshead speed 2.5 mm/min). The notch was placed within the inner span on the tensile side. The fracture resistance K_{ISB} was then calculated according to the model of Chantikul [19]. It must be considered, that indentation methods lead to overestimated fracture toughness values of macroscopic samples due to the influence of the transformation zone of the indenter itself under the indent. The phase analysis by XRD (Panalytical, NL, $CuK_\alpha 1$, graphite monochromator, Bragg-Brentano setup, accelerator detector) was carried out by measuring the intensities of -111 and 111 monoclinic peaks and 101 tetragonal peak in the fingerprint region between 27-33° of 2θ. The monoclinic fraction V_m was calculated from the intensity ratio using the calibration curve of Toraya [20]. The coincidence of cubic 111 and tetragonal 101 peak should be noted. V_m,polished was measured on the polished surface of entire disks, V_m,fractured was measured on flat fracture surfaces of 2 x 4 mm^2 area produced in ISB tests of pre-notched samples. The much lower signal intensity was compensated by prolonged measuring time (1 h vs. 7 min). The size, h, of the transformed zone was calculated according to Kosmac [21].

2.2. Micro cantilever preparation

The samples were ground and polished prior to the milling of the micro cantilevers in the FIB. Former studies investigated the influence of FIB-induced damage by Ga-Ions on the fracture toughness. According to the literature no influence of the fracture toughness could be observed due to the Ga-preparation compared to macroscopic tests [22–24]. The sample surface was oriented in a Zeiss Crossbeam 540 FIB at an angle of 54° to the electron beam and 90° to the ion beam. The cantilevers were positioned close to the almost 90° polished edge of the sample. To investigate the fracture toughness as a function of size, micro cantilevers with lengths of 10, 70, 200 and 250 µm were milled. For the large cantilevers of 200 and 250 µm, the first coarse milling step was carried out at the (Bayerisches Laserzentrum, Erlangen, Germany) with a picosecond laser with 532 nm wavelength, a frequency of 8 kHz for 12 ps and 250 repeats. Further preparation of the large cantilevers and first milling steps of the medium and small sized cantilevers were performed with the FIB with a high current Ga^+-ion beam of 15 nA–65 nA at 30 kV. Further preparation included polishing the top of the cantilever to acquire a smooth surface for the notch and the undercutting of the lamella, resulting in a freestanding cantilever. Initial crack notches were milled over the whole breadth (B) in the surface with currents of 20 pA to 30 nA, depending on the width (W) of the cantilevers. The ratio of the initial crack length (a) to the width is about 0.2 - 0.3 a/w. Further thinning from both sides and the bottom are performed with currents of 700 pA to 3 nA, depending on the size of the final dimensions. An overview of the finished cantilevers in different dimensions is given in Fig. 1.

2.3. Micro cantilever testing techniques

The fracture toughness of the smallest micro cantilevers with a length of 10 µm was determined by in-situ bending with a force measurement system FMS-EM (Kleindiek Nanotechnik, Germany) inside the SEM. The FMS-EM system consists of a micromanipulator MM3A-EM and a force sensitive cantilever with a piezoresistive coating. The load was applied manually during the experiments up to a maximum force of about 360 µN. A video is recorded during the experiment to track the displacement of the cantilever by digital image correlation and to consider the shifting of the indenter tip during bending. DIC was performed to evaluate the force-displacement curve with the software Veddac 5.1 from (Chemnitzer Werkstoffmechanik GmbH, Germany). The fracture toughness K_{Ic} is calculated from the maximum force during loading and the dimension of the cantilever according to the formula:

$$K_{IC} = \frac{F_c L}{B W^{3/2}} Y\left(\frac{a}{w}\right) \quad (1)$$

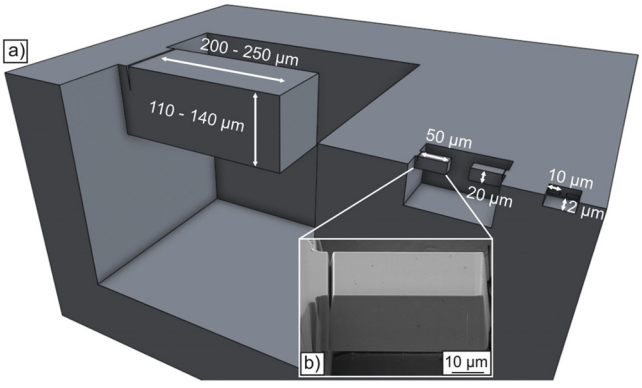

Fig. 1. a) Schematic figure of micro cantilevers in varying dimensions with the length of 10, 50 and 200–250 µm. The large cantilevers (50 & 200–250 µm) were tested ex-situ, the smaller ones (10 µm) in-situ. b) SEM image of a 50 µm micro cantilever.

For brittle materials with no plastic deformation F_c is the maximum load at which the cantilever fails and L is the distance between the loading position of the indenter tip and the notch. Y is a geometric function that depends on the ratio of the initial crack length (a) and the width (w) of the cantilever [11,25]. To calculate the plane strain fracture toughness K_{IC} at the micro scale, macroscopic standards cannot be fulfilled [26,27]. Therefore the subscript "Q" for K_{IQ} is used as suggested by Ast et al. [12]. This indicates that the fracture toughness is a "conditional" value. Regarding the plastic part of the fracture toughness, the J-Integral introduced by Rice [28] according to the iterative method given in the ASTM 1820 [27] was used:

$$J_{(i)} = J_{(i)}^{el} + J_{(i)}^{pl} \tag{2}$$

$$= \frac{(K_{IQ,(i)})^2(1-\nu^2)}{E} + \left[J_{(i-1)}^{pl} + \frac{\eta(A_{(i)}^{pl} - A_{(i-1)}^{pl})}{B(W-a_{(i-1)})}\right]\left[1 - \frac{a_{(i)} - a_{(i-1)}}{W - a_{(i-1)}}\right] \tag{3}$$

J consists of J^{el} and J^{pl} which represent the elastic and plastic values of the J-integral for each iterative step i, J^{el} is described by the Young's modulus E and the Poisson's ratio ν of the material. The dimensionless number η is equal to two for plane strain state [27] and the plastic work A^{pl} was computed numerically from the load displacement curves for each point, subtracting the elastic work either by using the initial loading slope k or by calculating it from the cantilever stiffness. It must be considered that plain strain conditions were presumed for all cantilevers. But plain strain conditions were not given for the smallest cantilevers due to the small dimensions.

The plastic deformation, as it occurs in Y-TZP, when the initial crack starts to propagate unstable, has to be taken into account with the J-Integral. To determine the fracture toughness K_{IQ} at the beginning of instable crack growth, from the critical J-Integral J_Q, the following equation was used.

$$K_{IQ,J} = \sqrt{\frac{J_Q E}{1-\nu^2}} \tag{4}$$

For the determination of J-Integral also the yield stress (σ_y) of the material must be known. According to Tabor et al., a conservative assumption for the yield stress is, that the yield stress is about 1/3 of the Vickers hardness (HV10) [29]. Kern et al., determined the Vickers hardness (HV10) of 3Y-TZP sintered at 1300 °C for 1 h as it was investigated in this study about 1230 HV [9]. Therefore a conservative assumption of the yield stress of about 4000 MPa can be expected. The expected process zone can be calculated by the following equation:

$$a,\ B,\ (W-a) = 2{,}5\left(\frac{K_{IC}}{\sigma_y}\right) \tag{5}$$

According to the macroscopic fracture toughness of 8.5 $MPam^{1/2}$ and a yield stress of about 4000 MPa the cantilevers must have a remaining width of more than 11.2 µm to fulfill the plain strain conditions. Despite the smallest cantilevers this is the case for all bending experiments.

The medium and large sized cantilevers were tested ex-situ in a Nanoindenter G200 from *Agilent*, due to the necessity of higher loads. Tests were carried out in a displacement controlled setup via feedback loop. Harmonic contact stiffness was measured with a CSM (continuous stiffness mode) signal according to Ast et al. and Webler et al. [12,13]. A wedge indenter with a length of 20 µm is used for the medium sized cantilevers and 150 µm for the largest cantilevers for better positioning and to achieve torsion free bending. The wedge indenter had an opening angle of 120° and a peak tip rounding of about 2 µm.

2.4. Raman spectroscopy

Raman spectra of the fracture surfaces of the tested cantilevers were acquired using a 532 nm wavelength Nd-YAG laser microRaman with a 100X objective, a pinhole aperture of 25 µm resulting in an approximately 1 µm lateral resolution. Ten successive measurements with 30 s integration time each were performed on a Nicolet Almega XR Raman spectrometer from *Thermo Fischer Scientific*. A pattern of 8 × 8 spot measurements were performed to acquire the Raman mappings. The given spectra were first corrected by a baseline correction of a 5th degree polynomial and afterwards normalized with respect to the area of each spectra. For a qualitative determination of the t-ZrO_2 to m-ZrO_2 phase transformation, the monoclinic peak at 178 cm^{-1} is shown as an intensity based heat map for different samples and sintering temperatures.

Table 1
Mechanical properties and phase composition of polished and fractured surfaces.

		1300 °C/1 h/ 50MPa		1375 °C/1 h/ 50MPa		1450 °C/1 h/ 50MPa	
Property	Unit	Mean value	2σ	Mean value	2σ	Mean value	2σ
HV10	[GPa]	12.1	0.2	12.7	0.2	13.1	0.2
E	[GPa]	211	4	211	4	213	3
K_{DCM}	[$MPam^{1/2}$]	8.7	0.5	6.4	0.8	4.7	0.2
K_{ISB}	[$MPam^{1/2}$]	10.7	0.3	8.5	1	5.5	0.2
$V_{m,polished}$	[%]	6.8	1	5	1	5.7	1
$V_{m,fractured}$	[%]	45.2	2	30	2	26.3	2
h	[µm]	1.53	–	0.83	–	0.67	–

3. Results and discussion

3.1. Macroscopic reference samples

The mechanical properties and phase compositions of macroscopic samples in polished and fractured conditions after different sintering procedures are listed in Table 1.

As all materials are fully dense (ρ > 6.05 g/cm^3), the Young's modulus shows only insignificant changes. The rise of the Vickers hardness with increasing sintering temperature is in line with an earlier publication [9]. The same is true for the evolution of the fracture toughness and transformability. The comparison between the direct crack length measurement DCM (Niihara PQ model [17]) and the indentation strength in bending, ISB, test [19] indicate a more pronounced R-curve behavior in the long crack regime for the tougher materials. It should be noted that the fracture resistance of such "coated" 3Y-TZP material follows an s-shaped trend with a sharp drop in toughness at intermediate temperature. Using the given starting powder, this change is sharpest at the sintering temperature of 1375 °C which explains the higher standard deviation of values in the intermediate sintering temperature regime [9]. The transformability ($V_{m,fractured} - V_{m,polished}$) reflects the change in transformation toughness and is qualitatively in-line with measured fracture toughness.

3.2. Micro cantilever experiments

Fig. 2a) shows the stress intensity factor $K_{I,J}$ versus the relative displacement for micro cantilevers with a length of 10 up to 250 µm. This plot was chosen to show and compare the curves for cantilever bending tests with huge differences in force and displacement. This graphic presentation was used by Ast et al. in former studies [12]. A difference in the force-displacement curves according to the cross sections of the cantilevers was revealed. For the smallest cantilevers typical brittle failure with a linear curve with no bending or stable crack growth could be observed. With increasing the cantilever dimensions a bending of the last part of the force-displacement curves occurred. For the largest cantilevers the force-displacement curves showed a non-

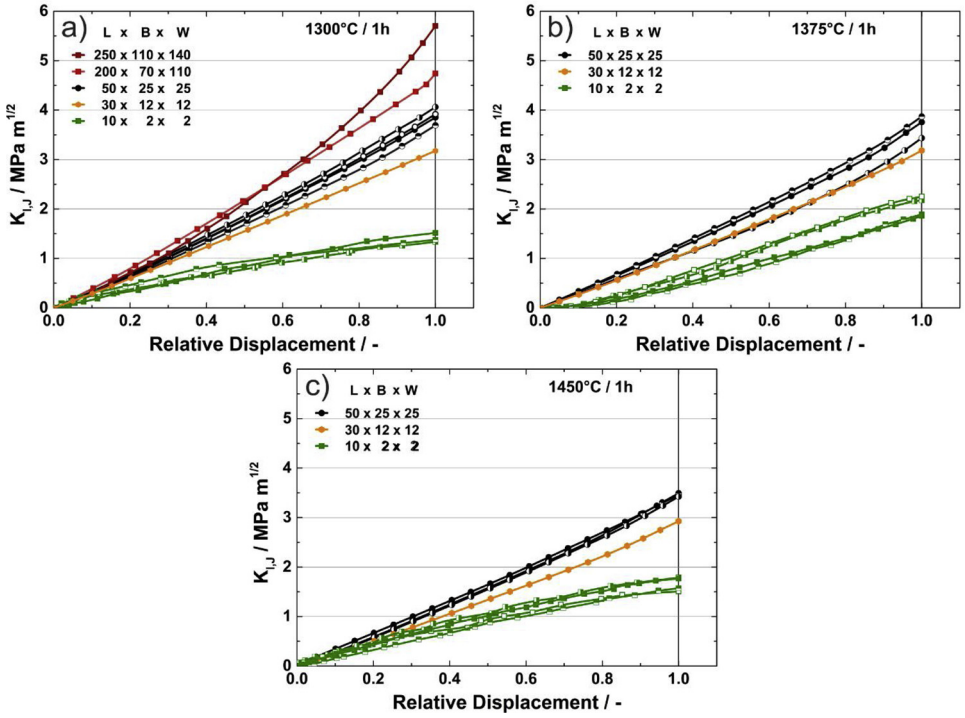

Fig. 2. Stress intensity factor $K_{I,J}$ over relative displacement curves for micro cantilevers in various dimensions of 3Y-TZP sintered for 1 h at a) 1300 °C b) 1375 °C and c) 1450 °C.

linearity range of about 400–500 nm before catastrophic failure. This size dependent non-linear range indicated stable crack growth by plastic deformation, which is according to references attributed to phase transformation during bending. The fracture toughness of the small cantilevers is about 1.3-1.5MPam$^{1/2}$ and thus significantly lower in comparison to macroscopic tests, where coprecipitated Y-TZP shows a fracture toughness of about 4.4 MPam$^{1/2}$ determined by three and four point single etched notched beam experiments (SENB) [30,31]. The small scatter of the results represent the reproducibility and reliability of the testing technique. The lower fracture toughness occurs due to the small fracture surface area, in which the formation of a transformation zone of sufficient size is suppressed. Furthermore it is assumed, that the tetragonal to monoclinic transformation is counteracted by the crack opening effect according to the volume expansion and therefore lowering the fracture toughness. This crack promoting effect lead to a fracture toughness even lower than the intrinsic fracture toughness of the material. According to McMeeking [14] we can assume full development of the transformation toughening effect at a crack extension a_s of 5 h. With the values from Table 1 a_s is estimated as 3.5–7.5 µm, which is larger than the height of the smallest cantilever (2 µm). It can thus be concluded that in case of the smallest cantilever, transformation toughening effect is not expected even for the most transformable 3Y-TZP sintered at 1300 °C. Furthermore no plain strain condition was given for the smallest cantilevers, affecting the J-Integral. Due to the lack of plasticity and the linear force-displacement curves this was negligible. Therefore the $J_{(i)}^{pl}$ part is almost zero and the fracture toughness determined by the J-Integral is equal to the fracture toughness determined by linear elastic fracture mechanics. A toughening effect should only occur in micro cantilevers that are longer than 10 µm. The toughening effect of the stress-induced tetragonal to monoclinic transformation is counteracted by the crack opening effect of the transformation related volume expansion, which for the smallest samples may promote rather than hinder crack propagation. Besides the intrinsic matrix toughness of the material no additional resistance to crack growth is present in these small samples. In medium sized cantilevers at least some additional toughening effect may occur, which results in a significantly higher fracture toughness of about 3.7-4.1MPam$^{1/2}$. Similar to the small in-situ tested samples, the scatter of ex-situ experiments was also very small. Further increasing of the cantilever dimensions led to an even higher fracture toughness. The K_{Ic} value raised to 4.7-5.7MPam$^{1/2}$ for the laser pre-milled cantilever. The remaining width (65–105 µm) after milling the notch provided enough volume for the transformation toughening effect to come into play. The dimensional requirements of the J-Integral to be calculated correctly was given for all experiments. With a J-Integral of 132 N/m the calculated minimum width of the largest cantilever had to be larger than 0.33 µm. All cantilevers met the J-Integral requirements even if macroscopic fracture toughness values are applied. The fracture toughness of specimens sintered at 1375 °C and 1450 °C for 1 h were also investigated, see Fig. 2b) and c). Micro cantilevers with the smallest geometry of 10 × 2 x 2 µm showed an almost equal fracture toughness compared to the 1300 °C specimen of about 1.5-1.8MPam$^{1/2}$. The small differences of the fracture toughness of specimens sintered at 1375 °C and 1450 °C in comparison to 1300 °C can be attributed to influence of grain orientation, grain size or measurement uncertainties. Cantilevers larger than 30 × 12 x 12 µm showed a decrease of the fracture toughness with increasing sintering temperature, which is qualitatively inline with the results obtained on macroscopic samples. Samples sintered at higher temperature show lower transformability and thus require smaller transformation zones to develop maximum toughness (which is, however at a much lower absolute level). It can therefore be understood that the increase of cantilever size has less effect on the maximum toughness of the specimen sintered at 1450 °C. They reach a toughness of 3.3-3.5MPam$^{1/2}$ for medium sized micro cantilevers. Fig. 3 shows the fracture toughness of the micro cantilever in different widths at all sintering temperatures.

3.3. Fracture surface after the micro cantilever bending experiments

Fig. 4 shows the fracture surfaces of micro cantilevers tested in in- and ex-situ bending experiments. A homogenous initial crack length over the whole breadth could be achieved for the smallest, Fig. 4a), and

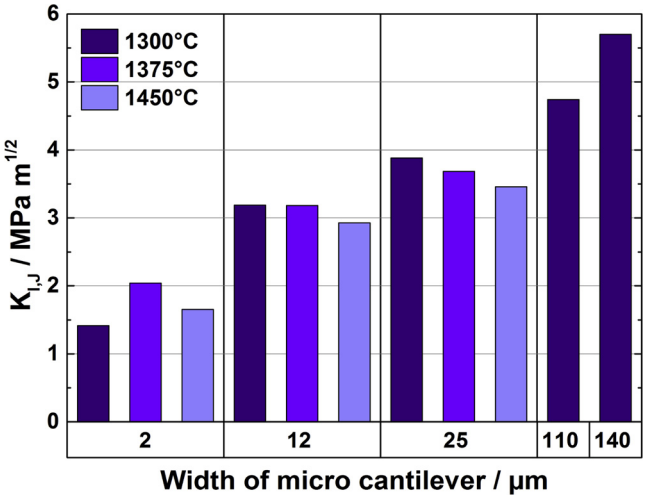

Fig. 3. Average fracture toughness of micro cantilevers with widths of 2–140 µm sintered at 1300 °C, 1375 °C and 1450 °C.

the largest, Fig. 4b), cantilever dimensions. Typical brittle fracture surfaces analogous to macroscopic fracture experiments were observed, with a grain size in the range of 90–110 nm after sintering at a temperature of 1300 °C for 1 h. Embedded in the fine grained matrix of tetragonal grains, larger cubic phases with a diameter between 1.1–2.2 µm randomly distributed over the fracture surface can be seen in Fig. 4c). This is in-line with previous publications [9,32]. For the fracture surfaces of the smallest cantilevers no cubic grains could be observed due to the small cross section of just 1.5 x 2 µm. Therefore the fracture toughness is not influenced by even lower fracture toughness of the cubic phase [33]. Similar microstructures were observed for samples, sintered at 1375 °C and 1450 °C. No significant difference of the fracture surfaces or plastic deformed regions near the initial crack could be seen.

3.4. Analysis of fracture surfaces with Raman spectroscopy

In order to quantify and locate phase transformation in 3Y-TZP, Raman spectroscopy was performed on micro cantilevers of specimens sintered at 1300 °C and 1450 °C. The fracture surfaces were positioned perpendicular to the Raman laser. Fig. 5 shows mappings with 8 × 8 spot measurements indicating the stress induced transformed monoclinic phase content over the complete fracture surface.

It can be seen that no monoclinic phase is found in the area of the initial crack at the top of the mappings. The amount of 5–6 vol.-% monoclinic phase measured by XRD is probably below the resolution threshold of the spectrometer. Below the notch, the fracture surface of the specimen sintered at 1300 °C shows an increase of the monoclinic phase content. The red areas show regions with a higher fraction of m-ZrO_2, Fig. 5a). Possible reasons for the asymmetric distribution could be due to that the wedge indenter was not perfectly aligned at the beginning of the bending experiments, resulting in a slightly higher stress on the right side of the cantilever. Nevertheless it is obvious, that the fracture surface of the micro cantilever after 1450 °C, Fig. 5b), showed much less monoclinic phase than the cantilever of the 1300 °C heat-treated material. This is in agreement with XRD results obtained on fracture surfaces of macroscopic samples [9]. At the bottom of both cantilevers almost no monoclinic phase was measurable. After a stable crack propagation, the remaining approximately 30% of the sample height shows no indication (1450 °C) or drastically reduced phase transformation (1300 °C) as almost no monoclinic phase was observed by Raman. This fact cannot be easily explained as *a priori* there is no obvious reason why the phase transformation should suddenly stop as long as the critical stress is applied. Moreover it is commonly believed that the martensitic transformation happens at the speed of sound and therefore cannot be surpassed by the crack [1]. It should, however, be considered that the effect is observed at the compressive side of the bar and that here failure happens at maximum crack velocity. It may be that the elastic response of the material is too slow and that for this reason only reduced transformation is observed. Another possible (but not very likely) explanation could be reversible transformation [34]. In any case this effect deserves some further investigations. Fig. 5c) compares the Raman spectra for the three points marked in Fig. 5a) and b). It can be seen, that in the region of the initial crack, illustrated by spectrum 1, no monoclinic phase but just peaks for the tetragonal phase at 146 cm^{-1} and 260 cm^{-1} was observed, confirming investigations of Kim et al. [35]. In contrast to that, spectrum 2 shows a significant increase in the monoclinic phase content with peaks at 181 cm^{-1} and 190 cm^{-1}. The Raman spectra for the specimen sintered at 1450 °C, however reveal less monoclinic phase compared to the specimen sintered at 1300 °C. The Raman analysis of the fracture surfaces confirmed the differences in the fracture behavior based on the stress induced martensitic transformation of tetragonal to monoclinic zirconia, previously measured with micro cantilever bending experiments.

4. Conclusion

Downscaling of specimen 3Y-TZP size for fracture toughness tests showed a clear interrelation between the size of the initial transformation zones, their ability to expand and to form a fully developed process zone and the size of the test specimen. The cantilever size effect is stronger pronounced the more transformable the TZP materials are. For the smallest cantilever diameters of ˜2 µm no differentiation between TZP materials of high transformability was detected. This is due to the fact that the initial zone sizes are in the range of the cantilever cross section. Larger cantilevers offer more space for the zone to expand. The measured toughness is considerably higher and scales with cantilever size. However, the plateau toughness value observed in macroscopic samples was not reached. The different transformabilities of TZP materials found by XRD in macroscopic samples was confirmed at fracture surfaces of small micro cantilevers by Raman mapping. In small samples in which the transformation zone is in the same order of

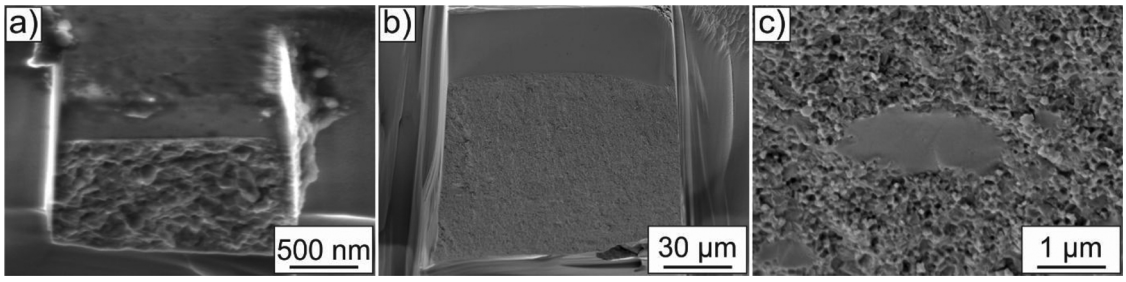

Fig. 4. Fracture surfaces of micro cantilevers sintered at 1300 °C for 1 h after bending experiments with fracture areas of a) 2 x 2 µm, b) 110 x 140 µm and c) cubic phases randomly distributed in finer grain sized matrix.

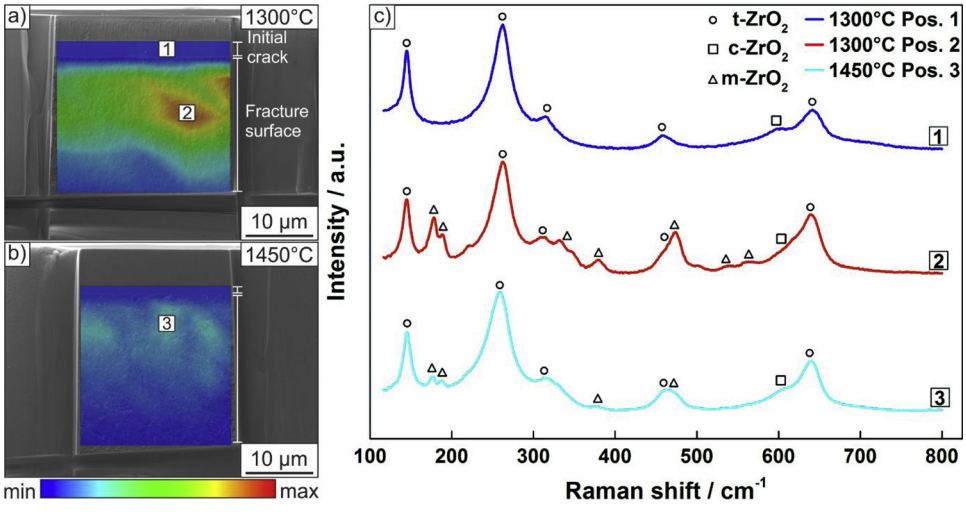

Fig. 5. Fracture surfaces of micro cantilevers sintered for 1 h at a) 1300 °C and b) 1450 °C, after bending experiments with a fracture area of 25 x 25 µm. The heat map indicates qualitatively the amount of the m-ZrO_2-phase with the min. (blue) and max. (red). c) Three Raman spectra showing the individual spectra for the three positions (1–3) shown in a) and b). (For interpretation of the references to colour in this figure legend, the reader is referred to the web version of this article).

magnitude as the sample dimension the crack opening effect of the transformation related volume expansion cannot be neglected as it adds an additional crack-opening stress intensity increment. This may be the reason why small samples do not even reach the intrinsic toughness of zirconia at the crack tip (K_{tip} = 4 $MPam^{1/2}$). In larger samples this crack opening increment is compensated by the bulk which provides the necessary rigidity. The inefficiency of transformation toughening to increase the damage tolerance of parts of very small dimensions has strong implications to engineering of miniaturized zirconia components. Not only does the enhanced transformability limit maximum strength, if the sample size is too small to allow development of a transformation zone and if the backing is not stiff enough to let the crack closing compressive stresses exerted by the transformation related volume expansion to come into effect. It can be even suspected that if the backing is too small, the transformation process even leads to a crack opening contribution and to a lowering of the actual toughness below the value of the crack tip toughness in a bulk 3Y-TZP material.

Acknowledgements

The authors would like to acknowledge Dr. Kristian Cvecek from the bayerischen Laserzentrum in Erlangen for providing picosecond laser fabrication of micro cantilever. The authors are grateful for providing Raman spectroscopy measurements at WW3 Institute of Glass and Ceramics at the University of Erlangen-Nürnberg. C. A. Macauley acknowledges financial support by the Bavarian Ministry of Economic Affairs and Media, Energy and Technology for the joint projects in the framework of the Helmholtz Institute Erlangen-Nürnberg for Renewable Energy (IEK-11) of Forschungszentrum Jülich.

References

[1] P.M. Kelly, L.R. Francis Rose, The martensitic transformation in ceramics — its role in transformation toughening, Prog. Mater. Sci. 47 (2002) 463–557, https://doi.org/10.1016/S0079-6425(00)00005-0.
[2] F.G. Marro, R.K. Chintapalli, A. Mestra, M. Anglada, Determination of the Intrinsic Fracture Toughness from the Cod Analysis of Indentation Cracks in Spark Plasma Sintered 3Y-TZP Reinforced with MWCNT, in: Spain, (2012) p. 6.
[3] R.H.J. Hannink, P.M. Kelly, B.C. Muddle, Transformation toughening in zirconia-containing ceramics, J. Am. Ceram. Soc. 83 (2000) 461–487, https://doi.org/10.1111/j.1151-2916.2000.tb01221.x.
[4] J. Kelly, I. Denry, Stabilized zirconia as a structural ceramic: an overview, Dent. Mater. 24 (2008) 289–298, https://doi.org/10.1016/j.dental.2007.05.005.
[5] M. Chen, B. Hallstedt, L. Gauckler, Thermodynamic modeling of the ZrO2–YO1.5 system, Solid State Ion 170 (2004) 255–274, https://doi.org/10.1016/j.ssi.2004.02.017.
[6] K. Matsui, H. Yoshida, Y. Ikuhara, Review: microstructure-development mechanism during sintering in polycrystalline zirconia, Int. Mater. Rev. 63 (2018) 375–406, https://doi.org/10.1080/09506608.2017.1402424.
[7] R. Singh, C. Gill, S. Lawson, G.P. Dransfield, Sintering, microstructure and mechanical properties of commercial Y-TZPs, J. Mater. Sci. 31 (1996) 6055–6062, https://doi.org/10.1007/BF01152158.
[8] C. Piconi, W. Burger, H.G. Richter, A. Cittadini, G. Maccauro, V. Covacci, N. Bruzzese, G.A. Ricci, E. Marmo, Y-TZP ceramics for artificial joint replacements, Biomaterials 19 (1998) 1489–1494, https://doi.org/10.1016/S0142-9612(98)00064-7.
[9] F. Kern, H. Strumberger, R. Gadow, Effects of Stabilizer Content and Sintering Conditions on Y-TZP Ceramics made from Stabilizer-Coated Nanopowders, (2017), https://doi.org/10.4416/JCST2017-00049.
[10] M. Turon-Vinas, J. Morillas, P. Moreno, M. Anglada, Evaluation of damage in front of starting notches induced by ultra-short pulsed laser ablation for the determination of fracture toughness in zirconia, J. Eur. Ceram. Soc. 37 (2017) 5127–5131, https://doi.org/10.1016/j.jeurceramsoc.2017.07.006.
[11] F. Iqbal, J. Ast, M. Göken, K. Durst, In situ micro-cantilever tests to study fracture properties of NiAl single crystals, Acta Mater. 60 (2012) 1193–1200, https://doi.org/10.1016/j.actamat.2011.10.060.
[12] J. Ast, T. Przybilla, V. Maier, K. Durst, M. Göken, Microcantilever bending experiments in NiAl – evaluation, size effects, and crack tip plasticity, J. Mater. Res. 29 (2014) 2129–2140, https://doi.org/10.1557/jmr.2014.240.
[13] R. Webler, M. Krottenthaler, S. Neumeier, K. Durst, M. Göken, Local fracture toughness and residual stress measurements on NiAl bond coats by micro cantilever and fib-based bar milling tests, Superalloys (2012) 93–102.
[14] R.M. McMeeking, A.G. Evans, Mechanics of transformation-toughening in brittle materials, J. Am. Ceram. Soc. 65 (1982) 242–246, https://doi.org/10.1111/j.1151-2916.1982.tb10426.x.
[15] B. Budiansky, J.W. Hutchinson, J.C. Lambropoulos, Continuum theory of dilatant transformation toughening in ceramics, Int. J. Solids Struct. 19 (1983) 337–355, https://doi.org/10.1016/0020-7683(83)90031-8.
[16] Z.X. Yuan, J. Vleugels, Preparation of Y2O3-coated ZrO2 powder by suspension drying, J. Mater. Sci. Lett. 19 (2000) 359–361.
[17] K. Niihara, A fracture mechanics analysis of indentation-induced Palmqvist crack in ceramics, J. Mater. Sci. Lett. 2 (1983) 221–223, https://doi.org/10.1007/BF00725625.
[18] K. Niihara, R. Morena, D.P.H. Hasselman, Evaluation of KIc of brittle solids by the indentation method with low crack-to-indent ratios, J. Mater. Sci. Lett. 1 (1982) 13–16.
[19] P. Chantikul, G.R. Anstis, B.R. Lawn, D.B. Marshall, A critical evaluation of indentation techniques for measuring fracture toughness: II, strength method, J. Am. Ceram. Soc. 64 (1981) 539–543, https://doi.org/10.1111/j.1151-2916.1981.tb10321.x.
[20] H. Toraya, M. Yoshimura, S. Somiya, Calibration curve for quantitative analysis of the monoclinic-tetragonal ZrO2 system by X-ray diffraction, J. Am. Ceram. Soc. 67 (1984) C-119–C-121, https://doi.org/10.1111/j.1151-2916.1984.tb19715.x.
[21] T. Kosmać, R. Wagner, N. Claussen, X-ray determination of transformation depths in ceramics containing tetragonal ZrO2, J. Am. Ceram. Soc. 64 (1981) c-72–c-73, https://doi.org/10.1111/j.1151-2916.1981.tb10285.x.
[22] S. Wurster, C. Motz, R. Pippan, Characterization of the fracture toughness of micro-sized tungsten single crystal notched specimens, Philos. Mag. 92 (2012) 1803–1825, https://doi.org/10.1080/14786435.2012.658449.
[23] B.N. Jaya, C. Kirchlechner, G. Dehm, Can microscale fracture tests provide reliable fracture toughness values? A case study in silicon, J. Mater. Res. 30 (2015) 686–698, https://doi.org/10.1557/jmr.2015.2.
[24] K. Takashima, Y. Higo, Fatigue and fracture of a Ni-P amorphous alloy thin film on the micrometer scale, Fatigue Fract. Eng. Mater. Struct. 28 (2005) 703–710, https://doi.org/10.1111/j.1460-2695.2005.00923.x.
[25] K. Matoy, H. Schönherr, T. Detzel, T. Schöberl, R. Pippan, C. Motz, G. Dehm, A comparative micro-cantilever study of the mechanical behavior of silicon based passivation films, Thin Solid Films 518 (2009) 247–256, https://doi.org/10.1016/j.tsf.2009.07.143.
[26] ASTM International, ASTM Standard E399-90. Standard test method for plane strain

fracture toughness of metallic materials, Technical Report, Am. Soc. Test. Mater. Phila. PA, (1993).
[27] ASTM International, ASTM Standard E1820, standard test method for measurement of fracture toughness, Technical Report, ASTM Int., West Conshohocken PA U. S, 2013.
[28] J.R. Rice, A path independent integral and the approximate analysis of strain concentration by notches and cracks, J. Appl. Mech. 35 (1968) 379, https://doi.org/10.1115/1.3601206.
[29] D. Tabor, The hardness of solids, Rev. Phys. Technol. 1 (1970) 145–179, https://doi.org/10.1088/0034-6683/1/3/I01.
[30] T. Nose, T. Fujii, Evaluation of fracture toughness for ceramic materials by a single-edge-precracked-beam method, J. Am. Ceram. Soc. 71 (1988) 328–333, https://doi.org/10.1111/j.1151-2916.1988.tb05049.x.
[31] R.J. Roberts, R.C. Rowe, P. York, The measurement of the critical stress intensity factor (KIC) of pharmaceutical powders using three point single edge notched beam (SENB) testing, Int. J. Pharm. 91 (1993) 173–182, https://doi.org/10.1016/0378-5173(93)90337-F.
[32] F. Kern, Evidence of phase transitions and their role in the transient behavior of mechanical properties and low temperature degradation of 3Y-TZP made from stabilizer-coated powder, Ceramics 2 (2019) 271–285, https://doi.org/10.3390/ceramics2020022.
[33] J. Chevalier, L. Gremillard, A.V. Virkar, D.R. Clarke, The tetragonal-monoclinic transformation in zirconia: lessons learned and future trends, J. Am. Ceram. Soc. 92 (2009) 1901–1920, https://doi.org/10.1111/j.1551-2916.2009.03278.x.
[34] D.B. Marshall, M.R. James, Reversible stress-induced martensitic transformation in ZrO2, J. Am. Ceram. Soc. 69 (1986) 215–217, https://doi.org/10.1111/j.1151-2916.1986.tb07410.x.
[35] B.-K. Kim, J.-W. Hahn, K.R. Han, Quantitative phase analysis in tetragonal-rich tetragonal/monoclinic two phase zirconia by Raman spectroscopy, J. Mater. Sci. Lett. 16 (1997) 669–671.